Eur. Phys. J. C (2018) 78:425
https://doi.org/10.1140/epjc/s10052-018-5831-z

THE EUROPEAN PHYSICAL JOURNAL C

Regular Article - Theoretical Physics

Stop coannihilation in the CMSSM and SubGUT models

John Ellis[1,2,3], **Jason L. Evans**[4,a], **Feng Luo**[5], **Keith A. Olive**[6], **Jiaming Zheng**[7]

[1] Theoretical Particle Physics and Cosmology Group, Department of Physics, King's College London, Strand, London WC2R 2LS, UK
[2] National Institute of Chemical Physics and Biophysics, Rävala 10, 10143 Tallinn, Estonia
[3] Theoretical Physics Department, CERN, 1211 Geneva 23, Switzerland
[4] School of Physics, KIAS, Seoul 130-722, South Korea
[5] Kavli IPMU (WPI) UTIAS, The University of Tokyo, Kashiwa, Chiba 277-8583, Japan
[6] William I. Fine Theoretical Physics Institute, School of Physics and Astronomy, University of Minnesota, Minneapolis, MN 55455, USA
[7] Department of Physics, University of Tokyo, Bunkyo-ku, Tokyo 113-0033, Japan

Received: 15 February 2018 / Accepted: 21 April 2018 / Published online: 28 May 2018

Abstract Stop coannihilation may bring the relic density of heavy supersymmetric dark matter particles into the range allowed by cosmology. The efficiency of this process is enhanced by stop-antistop annihilations into the longitudinal (Goldstone) modes of the W and Z bosons, as well as by Sommerfeld enhancement of stop annihilations and the effects of bound states. Since the couplings of the stops to the Goldstone modes are proportional to the trilinear soft supersymmetry-breaking A-terms, these annihilations are enhanced when the A-terms are large. However, the Higgs mass may be reduced below the measured value if the A-terms are too large. Unfortunately, the interpretation of this constraint on the stop coannihilation strip is clouded by differences between the available Higgs mass calculators. For our study, we use as our default calculator `FeynHiggs 2.13.0`, the most recent publicly available version of this code. Exploring the CMSSM parameter space, we find that along the stop coannihilation strip the masses of the stops are severely split by the large A-terms. This suppresses the Higgs mass drastically for μ and $A_0 > 0$, whilst the extent of the stop coannihilation strip is limited for $A_0 < 0$ and either sign of μ. However, in sub-GUT models, reduced renormalization-group running mitigates the effect of the large A-terms, allowing larger LSP masses to be consistent with the Higgs mass calculation. We give examples where the dark matter particle mass may reach $\gtrsim 8$ TeV.

1 Introduction

Searches for supersymmetry [1,2] at the LHC have explored much of the theory space favoured previously in the context of simplified phenomenological models with universal soft super- symmetry-breaking parameters at an input GUT scale. However, in our opinions supersymmetry (SUSY) remains one of the most attractive options for physics beyond the Standard Model, since it facilitates grand unification of the gauge couplings [3–7] , improves the naturalness of the electroweak mass hierarchy [8–10] and plays an essential role in string theory. Moreover, the lightest supersymmetric particle (LSP) is an excellent cold dark matter candidate if R-parity is conserved [11,12], as we assume here. In addition, supersymmetry stabilizes the electroweak vacuum [13–15], can trigger electroweak symmetry breaking [16–21] and predicted successfully the mass of a Higgs boson with couplings similar to those in the Standard Model [22–30].

Therefore we are motivated to pursue the search for supersymmetry, and note that there are still regions of supersymmetric model space that the LHC has yet to explore, and may never reach. Some of the regions that are difficult to see at the LHC can be seen through indirect detection, and another promising avenue is the search for proton decay [31]. If the theory at the GUT scale is minimal SU(5), the Wilson coefficients of the dimension-5 proton-decay operators tend to be large, destabilizing the proton [32,33]. In general, unless $\tan\beta \lesssim 5$, the proton is unstable for a SUSY-breaking scale that can explain dark matter[1] [35,36]. However, in this work we ignore such constraints, assuming that the GUT-scale theory is either not minimal SU(5) or has some additional symmetry, such as a Peccei-Quinn symmetry, which enhances the proton lifetime. In this way, we are not hostages of some unknown high-scale dynamics.

[a] e-mail: jlevans@kias.re.kr

[1] Exceptions to this are models such as pure gravity meditation that have a large hierarchy between the sfermion and gaugino masses [34].

Instead of worrying about constraints that are dependent on the UV completion of the model, we take a phenomenological approach and focus on the regions of supersymmetric model space that has not yet been probed by the LHC. Included in these unexplored regions are strips of parameter space extending to larger masses where the thermal abundance of relic LSPs is brought down into the range allowed by the cosmological cold dark matter density measurements [37] via some enhancement of the conventional annihilation mechanism, such as rapid annihilation through heavy Higgs bosons or coannihilation with some other, nearly-degenerate supersymmetric particle(s) [38].

Examples of possible coannihilation partners include sleptons [39–47], electroweak inos [48–51], squarks [52–63] and gluinos [63–76]. Coannihilation of the LSP with the lighter stau slepton has been explored extensively, and is now almost excluded by LHC searches [46,47]. The cosmological cold dark matter density can be obtained via coannihilations with Higgsinos if the LSP mass $\sim$ 1 TeV [77,78], and by coannihilations with Winos if the LSP mass $\sim$ 3 TeV [79–82]. Much larger LSP masses, and hence much heavier sparticle spectra, are possible if the LSP coannihilates with strongly-interacting sparticles such as gluinos or stop squarks. Coannihilation with gluinos is not possible in models with universal gaugino masses at the GUT scale, though it is possible if this assumption is relaxed. On the other hand, coannihilation with stop squarks is possible in models with universal soft supersymmetry-breaking parameters, and is a scenario capable of raising the sparticle spectrum into the multi-TeV range and evading LHC searches [62].

The fact that stop coannihilation is such a promising scenario for reconciling a heavy supersymmetric spectrum with the attractive possibility that the LSP provides the cosmological relic density motivates the re-examination of this scenario, which we undertake in this paper. We consider in particular, various effects that tend to extend the stop coannihilation strip, including annihilations into longitudinal (Goldstone) components of the W and Z bosons, large trilinear soft supersymmetry-breaking A-terms, Sommerfeld enhancement [83–85] of stop annihilations [61,73,86], and the possible effects of bound states [87–96].

We pay particular attention to the limitations on the stop coannihilation strip imposed by the LHC measurement of the Higgs mass [97]. The interpretation of this constraint is sensitive to details of Higgs mass calculations with heavy sparticle spectra. These have been studied extensively recently, but still with significant differences between the available Higgs mass calculators [98–104]. Within the CMSSM [35,105–131], in which the soft supersymmetry-breaking scalar and gaugino masses are assumed to be universal at the GUT scale, we find using the most recent publicly available version of the FeynHiggs Higgs mass calculator, `FeynHiggs 2.13.0`, that the Higgs mass constraint is a severe limitation on the size of the LSP mass.

In addition to the CMSSM, we also consider its 'sub-GUT' generalization [35,131–135] in which universality of the soft supersymmetry-breaking parameters is imposed at a lower scale, as occurs in mirage unification models [136–147]. Sub-GUT models can have enhanced coannihilations of the LSP and the lighter stop into final states including W and Z bosons. This enhancement occurs because the masses of the left- and right-handed stop masses are more degenerate than in the CMSSM, as a consequence of the reduced renormalization-group running. With the masses less split, for any fixed value of $m^2_{\tilde{t}_1}+m^2_{\tilde{t}_2}$, the ratio $A_t^2/(m_{\tilde{t}_1}m_{\tilde{t}_2})$, important for the Higgs mass calculation, is decreased. Since the ratio $A_t^2/(m^2_{\tilde{t}_1}+m^2_{\tilde{t}_2})$ is important for determining the rate of stop-antistop annihilation into the longitudinal modes of the W and Z, the stop coannihilation strip can be extended in such sub-GUT models. Moreover, in certain regions of the parameter space of sub-GUT models, the masses have the special relationship $2m_{\tilde{t}_1} \simeq 2m_\chi \simeq m_H$, where $m_{\tilde{t}_1}$, m_χ and m_H are the lightest stop mass, LSP mass and heavy CP-even Higgs boson mass, respectively. In these regions, the stop-antistop annihilation rate is enhanced by resonance effects because $2m_{\tilde{t}_1} \simeq m_H$, amplifying the ability of stop coannihilation with the LSP to reduce the relic density, and the stop coannihilation strip is further extended. We give examples of sub-GUT scenarios where the dark matter particle mass may reach $\sim$ 7 TeV.

The layout of our paper is as follows. In Sect. 2 we discuss the impact of annihilations into longitudinal components of the W and Z on the extent of the stop coannihilation strip. In Sect. 3 we discuss the impact of bound states, showing how the longitudinal components of the gauge bosons enhance the decays of the bound states. In Sect. 4 we illustrate the importance of these effects in the CMSSM, discussing the potential impact of the Higgs mass constraint. In Sect. 5 we extend the analysis to sub-GUT models in which the stop masses are less split. In such a case, the Higgs mass is less suppressed and the stop coannihilation strip may extend to larger values of the LSP mass. Finally, Sect. 6 summarizes our conclusions.

2 The Goldstone equivalence theorem and stop coannihilation

The Goldstone Equivalence [148–150] theorem states that the longitudinal components of the gauge bosons of a broken symmetry retain the interactions they would have in the absence of gauge interactions, i.e., they interact as Goldstone bosons. If the interactions of the Goldstone bosons are large, they may enhance the interactions of the gauge bosons. The best-known example of this is $t \to W^+b$ decay. Naively, one

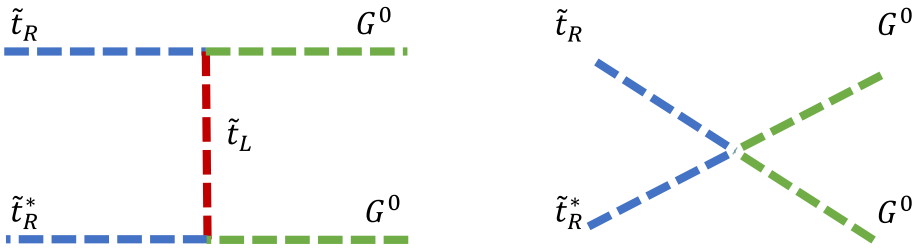

Fig. 1 Leading-order Goldstone-boson contributions to $\tilde{t}_R\tilde{t}_R^*$ annihilation

would have expected that the dominant contribution to this decay would be proportional to g_2^2, where g_2 is the SU(2) electroweak gauge coupling, since this appears to be a weak process. However, since the charged Goldstone boson in the Standard Model couples to t and b with a strength y_t, where y_t is the top Yukawa coupling that is larger than g_2, this decay is enhanced:

$$\Gamma_t \simeq \frac{g_2^2}{64\pi}\frac{m_t^3}{m_W^2} = \frac{y_t^2}{32\pi}m_t. \tag{1}$$

Similar behaviours are present in all scattering processes involving the W and Z. This type of enhancement turns out to be relevant when considering coannihilation processes involving the stop, as we see below.

Since the MSSM is a two-Higgs-doublet model, the Goldstone bosons are mixtures of states in the $H_{u,d}$ multiplets that give masses to the up- and down-type quarks:

$$H_u \supset \sin\beta \begin{pmatrix} G^+ \\ \frac{1}{\sqrt{2}}G^0 \end{pmatrix} \qquad H_d \supset -\cos\beta \begin{pmatrix} \frac{1}{\sqrt{2}}G^0 \\ G^- \end{pmatrix} \tag{2}$$

where $\tan\beta$ is the ratio of the two Higgs vevs, $G^\pm$ are the charged Goldstone bosons, and G^0 is the neutral Goldstone boson. Since we expect that $\tan\beta > 1$, $\cos\beta$ is generally small and the couplings of the components of the Goldstone bosons in the H_d multiplet are suppressed. On the other hand, the interactions of the components of the Goldstone bosons in the H_u multiplet can be quite large. Since the stop interacts with H_u, it can have a large coupling with the charged and neutral Goldstone bosons, especially for the larger values of $\tan\beta$ considered below.

Thus, the relevant interactions of the stop with the Goldstone bosons arise from its interactions with the H_u multiplet:

$$\begin{aligned} -\mathcal{L} \supset\ & y_t(A_t H_u + \mu H_d^\dagger)\tilde{Q}_L\tilde{t} \\ & + |y_t|^2\left(|\tilde{Q}_L|^2|H_u|^2 + |\tilde{t}|^2|H_u|^2|\right) . \end{aligned} \tag{3}$$

As we have already discussed, since $y_t > g_2$, these interactions are dominant in electroweak scattering processes for the stop. What is less obvious is that these are also more important than the scattering processes controlled by the strong coupling, g_3.

To show the significance of the scattering of stops into the longitudinal components of the W and Z,[2] we display the leading-order contribution to these processes. Calculating them requires the choice of a gauge. In unitary gauge, the Goldstone bosons disappear from the theory and become the longitudinal components of the gauge bosons, and it is difficult to see the origin of the enhancement to the scattering of the gauge bosons in this gauge, since the Goldstone bosons are not manifest. However, in the equivalent Feynman gauge, the Goldstone bosons *are* present explicitly and their contributions can quite easily be separated from other contributions. The most important contributions of the Goldstone bosons to the annihilation process $\tilde{t}_R\tilde{t}_R^*$ can be seen in Fig. 1,[3] with analogous diagrams for the charged Goldstone boson mode.

Using the interactions of the stop and Goldstone bosons found in (3), the dominant s-wave contribution to the thermally-averaged annihilation cross sections are found to be

$$\begin{aligned} \langle\sigma v\rangle_{\tilde{t}\tilde{t}^*\to W^+W^-} \simeq 2\langle\sigma v\rangle_{\tilde{t}\tilde{t}^*\to ZZ} \simeq \frac{g_2^4}{128\pi m_{\tilde{t}_R}^2}\left(\frac{m_t}{m_W}\right)^4 \\ \times\left(\frac{(A_t+\mu\cot\beta)^2 - m_{\tilde{t}_R}^2 - m_{\tilde{t}_L}^2}{m_{\tilde{t}_R}^2 + m_{\tilde{t}_L}^2}\right)^2 + \cdots , \end{aligned} \tag{4}$$

where the $\ldots$ represent contributions that are smaller by a factor $\mathcal{O}(m_W^2/m_t^2)$. As can be seen from this expression, there are two ways in which this process is enhanced. The first is because $m_t/m_W > 1$, which is the same enhancement found in the decay $t \to bW$, and the second is unique to scalars. Because A_t^2 can be larger than $m_{\tilde{t}_R}^2 + m_{\tilde{t}_L}^2$, there is an additional possible enhancement of this annihilation process. For $A_t^2 \gg m_{\tilde{t}_R}^2 + m_{\tilde{t}_L}^2$ the $\tilde{t}_R\tilde{t}_R^*$ annihilation rate is greatly increased, and the length of the stop coannihilation strip is significantly extended.

However, $|A_t|$ cannot be increased without bound. If $|A_t|$ becomes too large, one of the stop masses becomes tachyonic. This occurs when A_t is of order $\sim m_{SUSY}^2/v$. If such

[2] The significance of the Goldstone boson mode was also discussed in [151].

[3] There are also diagrams involving the Goldstone bosons that contribute to $\tilde{t}_R\tilde{t}_R^* \to G^0Z$, though their contributions to the $\tilde{t}_R\tilde{t}_R^* \to ZZ$ amplitude are suppressed by a factor of g_2, and can be neglected for the purposes of this discussion. However, all contributions to $\tilde{t}_R\tilde{t}_R^* \to ZZ$ are included in our numerical calculation.

a large value of A_t was allowed, the stop coannihilation trip would have no end.[4] However, if A_t is much larger than the soft supersymmetry-breaking scalar masses, small changes in the RG scale would lead to large changes in the soft masses. In the context of a UV-complete model, this suggests that the mass spectrum required at the input scale is rather contrived. Even more troubling, the mass of the SM-like Higgs boson becomes very sensitive to A_t when it is much larger than the stop masses. Indeed, as A_t is increased, the SM-like Higgs boson masses is driven to zero. For these reasons, it is expected that A_t cannot be much larger than the sfermion masses.[5] Even with this restriction on the size of A_t, the scattering cross section in (4) still gives an important boost to the stop-antistop annihilation rate.

The above restrictions constrain the amount of enhancement of the scattering cross section in (4) for the CMSSM. To maximize this enhancement, one may consider degenerate left- and right-handed stop masses. Such a degeneracy helps because the corrections that reduce the Higgs mass are $\propto A_t^2/(m_{\tilde{t}_R} m_{\tilde{t}_L})$, whereas the enhancement to the scattering cross section in (4) is $\propto A_t^2/(m_{\tilde{t}_R}^2 + m_{\tilde{t}_L}^2)$. The ratio of the enhancement in the scattering cross section to the reduction in the Higgs mass is therefore $\propto (m_{\tilde{t}_R} m_{\tilde{t}_L})/(m_{\tilde{t}_R}^2 + m_{\tilde{t}_L}^2)$, which is maximized when the $m_{\tilde{t}_{R,L}}$ are equal. A class of models that have more degenerate stop masses are sub-GUTs, in which the RG running of the masses is reduced. As we will see below, this increased degeneracy indeed leads to acceptable dark matter densities with larger LSP masses.

3 Bound-state effects in stop coannihilation

Another important effect that can lengthen the stop coannihilation strip is bound-state formation [75,76,94–96]. When dark matter froze out, at a temperature $T \sim m_{\tilde{t}}/25 \gg \Lambda_{QCD}$, QCD was a relatively long-range force, and strongly-interacting particles could form bound states. The formation rate of these states depends on the form of the long-range potential. For a non-Abelian force, the long-range potential takes the form

$$V(r) = -\frac{\xi}{r}, \tag{5}$$

where ξ is determined by Casimir coefficients, C_{X_1}, C_{X_2}, of the colour representations of the individual particles (X_1 and X_2) forming the bound state, as well as the combined Casimir coefficient of the two particles, $C_{X_1X_2}$:

$$\xi = \frac{1}{2}\left(C_{X_1} + C_{X_2} - C_{X_1X_2}\right)\alpha_s. \tag{6}$$

[4] This is due to the fact that the scattering cross section in Eq. (4) would scale as m_{SUSY}^2/v^4 instead of $1/m_{SUSY}^2$.

[5] When the Higgs mass is calculated using the code `FeynHiggs 2.13.0`, our default option, it generally provides a stronger constraint than does vacuum stability.

Since the gauge particle of a non-Abelian force is charged, if a gauge particle is emitted in the formation of the bound state, the Casimir of the bound state will in general be different from the combined Casimir of the initial-state particles. For example, a pair of SU(3) coloured particles in an octet configuration can transition to a bound state in a singlet representation via the emission of a gluon. If the cross section for the formation of these bound states is large, it alters how the constituents particles freeze out, which can be relevant when these coloured particles are coannihilating with a dark matter candidate.

The relevance of bound-state formation for coannihilation depends on whether or not the bound state, $\tilde{R}$, decays more quickly than it disassociates [75]:

$$\begin{aligned}\langle\sigma v\rangle_{\tilde{t}\tilde{t}^*\to \mathrm{SM}} &\to \langle\sigma v\rangle_{\tilde{t}\tilde{t}^*\, incl.\,\tilde{R}} \\ &\equiv \langle\sigma v\rangle_{\tilde{t}\tilde{t}^*\to \mathrm{SM}} + \langle\sigma v\rangle_{bsf}\frac{\langle\Gamma\rangle_{\tilde{R}}}{\langle\Gamma\rangle_{\tilde{R}} + \langle\Gamma\rangle_{dis}},\end{aligned} \tag{7}$$

where $\langle\sigma v\rangle_{bsf}$, $\langle\Gamma\rangle_{\tilde{R}}$, and $\langle\Gamma\rangle_{dis}$ are the thermally averaged formation cross section, decay rate and disassociation rate of the bound state, and $\langle\sigma v\rangle_{\tilde{t}\tilde{t}^*\to \mathrm{SM}}$ is the Sommerfeld-enhanced thermally-averaged cross section [61] excluding bound-state formation. If the bound state decays much more quickly than it disassociates, the bound state formation cross section contributes to the thermally-averaged cross section. Because the thermally-averaged cross section is increased by this process, the relic density is decreased for a given set of parameters and, thus, a cosmologically-acceptable relic density can be obtained for larger sparticle masses.

In the specific case of the stop, stop-antistop pairs can form bound states through the emission of a gluon. These bound states then decay to Standard Model particles. Since the decay rates of the bound states are related to the scattering rates of the corresponding particles, the impact of bound-state formation will be further enhanced by the dynamics of the Goldstone modes if decays of these bound states through the Goldstone components of the W/Z are dominant.

4 Stop coannihilation in the CMSSM

In this section we re-examine the stop coannihilation strip in the CMSSM for large A_0, paying close attention to the effects of annihilations to WW/ZZ and bound-state effects. We also examine the constraints on the extent of stop coannihilation strip imposed by the Higgs mass. However, because theoretical calculations of the Higgs mass are quite uncertain in this regime, we first examine the stop strip independently of the Higgs mass.

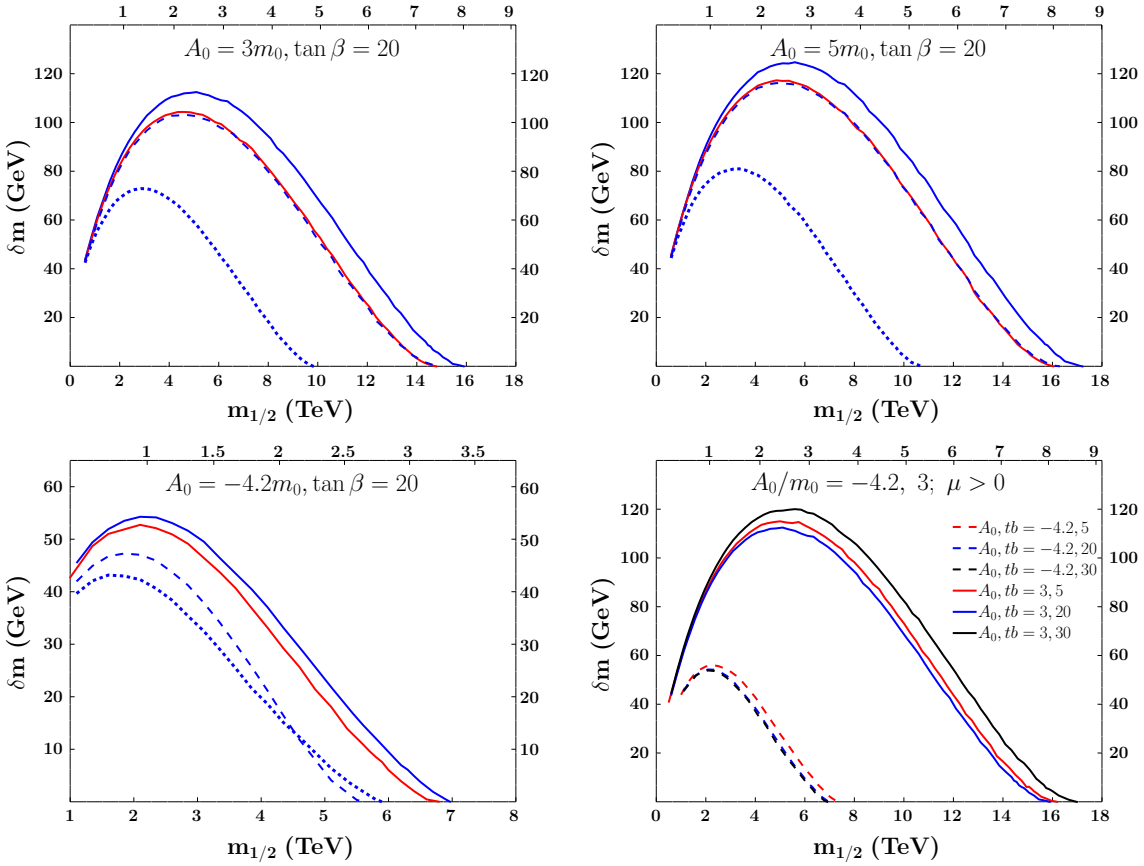

Fig. 2 The $\tilde{t}_1-$neutralino mass difference δm as a function of $m_{1/2}$ along the stop coannihilation strips in the CMSSM for $\tan\beta = 20$ with $A_0 = 3m_0$ (upper left panel), $A_0 = 5m_0$ (upper right panel) and $A_0 = -4.2m_0$ (lower left panel). The solid line includes both bound states and scatterings to WW/ZZ for $\mu > 0$ (blue) and $\mu < 0$ (red), the dashed line excludes only the bound-state effects, and the dotted line excludes only scatterings to WW/ZZ. The lower right panel compares results of $\tan\beta = 30$ (black), 20 (blue) and 5 (red) for $A_0 = 3m_0$ (solid lines) and for $A_0 = -4.2m_0$ (dashed lines) respectively.

4.1 The extent of the stop coannihilation strip

In order to understand the enhancements of the length of the stop coannihilation strip in the CMSSM due to annihilations to WW/ZZ and to bound-state effects, we use the SSARD code [104] to compute the particle mass spectrum and relic density. We study the stop coannihilation strip as a function of $m_{1/2}$ for various values of A_0 and both signs of the Higgsino mixing parameter μ. In each plot, the range of m_0 is not stated explicitly, but is chosen such that the lighter stop mass is nearly degenerate with the LSP, which is always the lightest neutralino, and generally the Bino.

In Fig. 2 we show the mass difference δm between the lighter stop and the LSP (left vertical axis) that gives the correct relic density as a function of $m_{1/2}$ (lower horizontal axis) and the corresponding values of the LSP mass, m_χ (upper horizontal axis), for $A_0 = 3m_0$ (upper left panel), $A_0 = 5m_0$ (upper right panel) and $A_0 = -4.2m_0$ (lower left panel), all with $\tan\beta = 20$, $\mu > 0$ with blue lines and $\mu < 0$ with red lines. The solid lines include both the bound-state effect and annihilations to WW/ZZ. The dashed lines exclude the bound-state effect and the dash-dotted lines exclude annihilations to WW/ZZ. As is clear from these panels, the annihilations to WW/ZZ are extremely important for large positive A-terms. This is due to the enhancement of annihilation to the longitudinal components of the W and Z discussed above. The bound-state effects, although less significant, also give an important boost to the extent of the stop coannihilation strip. Including both the WW/ZZ final states and bound-state effects, the stop coannihilation strip for $A_0 = 3m_0$, $\tan\beta = 20$ and $\mu > 0$ extends to $m_{1/2} \sim 16$ TeV, compared to < 10 TeV if the WW/ZZ final states are omitted, and < 15 TeV if bound-state effects are omitted. The corresponding numbers for $A_0 = 5m_0$ are $m_{1/2} \sim 17$ TeV, < 11 TeV and~ 16 TeV, respectively. The corresponding maximum values of m_χ when both these effects are included are ~ 8 and ~ 8.5 TeV, respectively.

If the sign of the A-term is flipped, the effect of the stop annihilations to ZZ/WW is diminished, as can be see in the lower left panel of Fig. 2, where we again plot the mass difference δm as a function of $m_{1/2}$ and m_χ for $A_0 = -4.2m_0$, $\tan\beta = 20$ and $\mu > 0$. This reduction in the effect of the scatterings to WW/ZZ is due to the RG running of the trilinear coupling A. For $A_0 < 0$, the gaugino and trilinear contribution to the trilinear beta function drives it towards zero. This leads to a more significant reduction in the A-term as it runs towards lower scales. With the A-term much smaller at the SUSY scale, the coupling of the Goldstone boson to the stop is diminished, and the scatterings to the longitudinal components of WW/ZZ are suppressed. The dominant stop-antistop annihilation channel is then $\tilde{t}\tilde{t}^* \to gg$. Since the annihilations to WW/ZZ are suppressed, the relic density tends to be much larger for $A_0 < 0$ for a comparable stop and LSP mass splitting, shortening the extent of the stop strip. The bound state effects for $A_0 = -4.2m_0$, on the other hand, are more significant than for the positive values of A_0 studied previously.[6] The length of the stop coannihilation strip for $A_0 = -4.2m_0$ extends to $m_{1/2} \sim 7$ TeV when both the WW/ZZ final states and bound-state effects are included, compared to $m_{1/2} < 6$ TeV if either of these are omitted, corresponding to $m_\chi \lesssim 3.5$ TeV.

A direct comparison between the lengths of the stop coannihilation strips for the different values of A_0 and different signs of μ when $\tan\beta = 20$ shows that the strip is shorter for smaller values of A_0, particularly for $A_0 < 0$. As can be seen in Eq. (4), μ also plays a role in the annihilations to WW/ZZ. The interaction of the stops with the Goldstone mode through μ is suppressed by $\cot\beta$, since this contribution stems from an interaction with H_d instead of H_u. However, even with this $\cot\beta$ suppression, it still plays a role. Comparing the results for $\mu > 0$ (blue lines) and $\mu < 0$ (red lines) in the upper panels and the lower left panel of Fig. 2, we see that the strip for $\mu < 0$ is ~ 1 TeV shorter than for $\mu > 0$ when $A_0 > 0$, with a smaller reduction for $A_0 = -4.2m_0$.[7] The corresponding reductions in the maximum values of m_χ are $\lesssim 0.5$ TeV.

Some comparisons of the lengths of the coannihilation strips for different values of $\tan\beta$ are shown in the lower right panel of Fig. 2. Those for $A_0 = 3m_0$ are shown as solid lines, and those for $A_0 = -4.2m_0$ are shown as dashed lines. The range in the extent of the stop coannihilation strip as a function $\tan\beta$ is of order $\Delta m_{1/2} \sim 1$ TeV for $A_0 = 3m_0$, namely between ~ 16 and 17 TeV, corresponding to $m_\chi \lesssim 8.5$ TeV. For $A_0 = -4.2m_0$, the range in the extent of the stop strip is considerably less, and for all values of $\tan\beta$ considered here the strip terminates at $m_{1/2} \sim 7$ TeV, corresponding to $m_\chi \lesssim 3.5$ TeV. We see that the strips are longest for $\tan\beta = 30$ (black lines) and $\tan\beta = 5$ (red lines) when $A_0/m_0 = 3$ and -4.2 respectively. For $\tan\beta = 5$, $\cot\beta$ is large enough that the μ contribution in Eq. (4) is important and extends the stop coannihilation strip a small but noticeable amount for both signs[8] of A_0. If $\tan\beta$ is further increased to 40, the LSP becomes a stau or a stop for both $A_0/m_0 = 3$ and -4.2.

4.2 The Higgs mass along the stop coannihilation strip

We now examine the constraints on the allowable extent of the stop coannihilation strip that are potentially imposed by the Higgs mass, comparing the results obtained using different codes for calculating M_h in the MSSM. The codes we consider in Figs. 3 and 4 are `FeynHiggs 2.10.0` (cyan lines) and[9] `2.13.0` (purple lines), `SSARD` (green lines) and `SUSYHD` (black lines).[10] `FeynHiggs 2.13.0` provides the choice of inputting parameters using either the on-shell (OS) scheme or the dimensional reduction (DR) scheme. We also compare in the figures the results obtained with these two different set of inputs, by converting the relevant parameters generated by the `SSARD` code to the OS scheme (purple solid lines) or DR scheme (purple dashed lines).

The two upper panels of Fig. 3 show stop coannihilation strips for $A_0 = -4.2m_0$, $\tan\beta = 5$ and $\mu > 0$ (left panel) or $\mu < 0$ (right panel), with the values of m_0 chosen to obtain the correct cosmological dark matter density, as calculated including WW/ZZ final states and bound-state effects. The values of $\delta m = m_{\tilde{t}_i} - m_\chi$ are shown as solid blue lines to be read on the left vertical axis. In these cases the values of M_h for identical inputs, to be read on the right vertical axis, have a spread $\lesssim 5$ GeV, which does not vary significantly along the strip, but is slightly larger for $\mu < 0$ than for $\mu > 0$. Similar results for $A_0 = -4.2m_0$, $\tan\beta = 20$ and $\mu > 0$ are shown in the middle left panel of the same figure, with M_h higher than the $\tan\beta = 5$ cases. Since `FeynHiggs 2.13.0` supersedes version `2.10.0` and it includes effects which are not part of other codes, we take it with on-shell input masses as our default in the following sections, with an uncertainty that we estimate to be at least 3 GeV.

[6] This is because the scattering rate in this regime is dominated by QCD interactions. Since bound state formation is also governed by QCD, it roughly doubles the annihilation cross section.

[7] This is due to the fact that this process is dominated by QCD processes for $A_0 < 0$.

[8] For $A_0 < 0$, we have $|\mu|\cot\beta > |A|$ which leads to an enhancement of the $\tilde{t}\tilde{t}^* \to WW$ scattering.

[9] The improvements included in FeynHiggs 2.13.0 are: three loop contributions to the RGE's including electroweak effects, threshold corrections are now correspondingly at the two-loop level, the top mass now includes two-loop QCD corrections and one-loop electroweak corrections, and upates to alleviate problems of scheme conversion.

[10] The `SSARD` calculation of M_h, is heavily based on the works in ref. [152–154] and is expected to be reasonably accurate only when the SUSY mass scales are $\gtrsim$ several TeV.

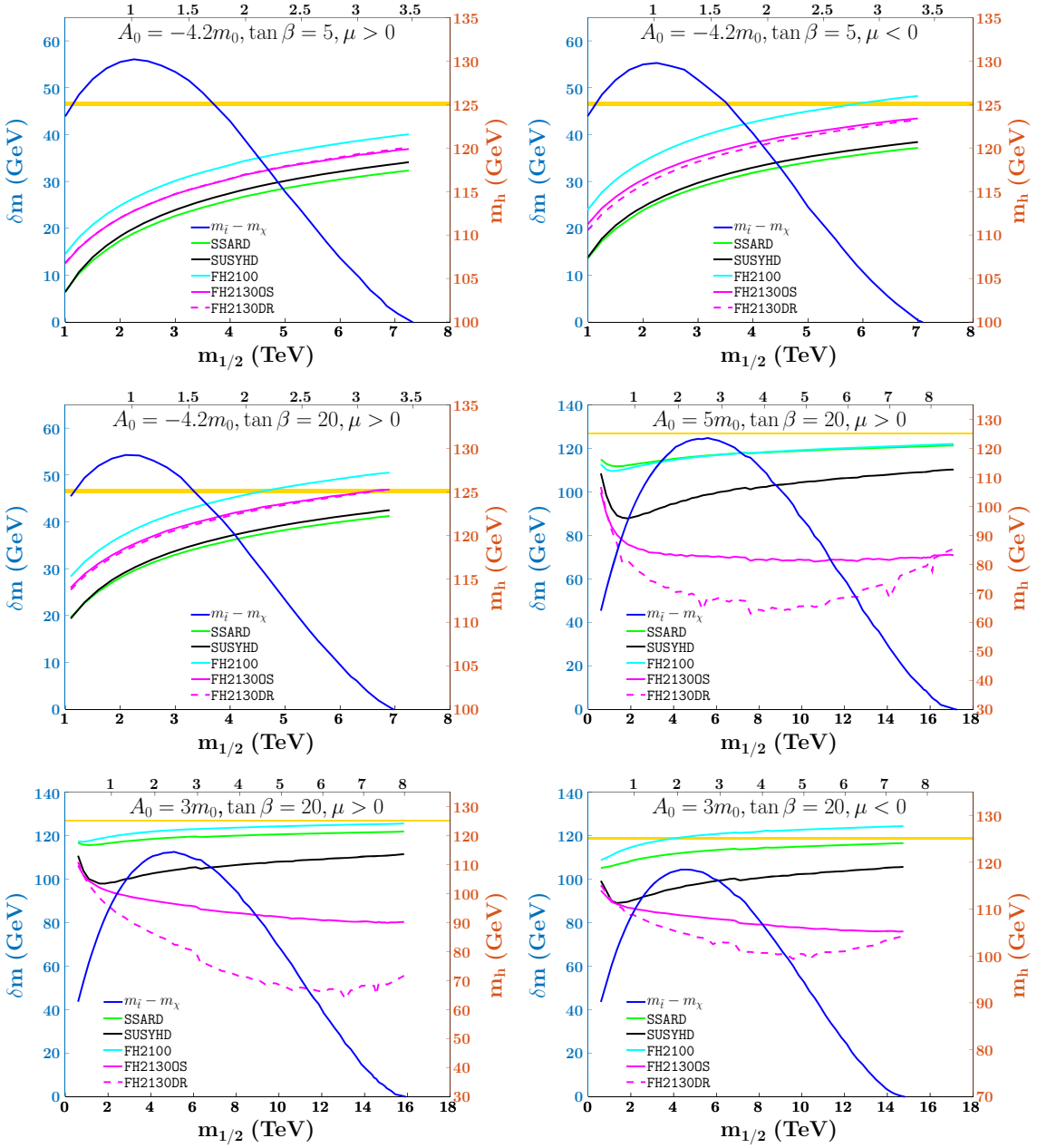

Fig. 3 The stop coannihilation strips for $A_0 = -4.2m_0$, $\tan\beta = 5$ and both positive or negative μ (upper panels), for $A_0 = -4.2m_0$, $\tan\beta = 20$ and $\mu > 0$ (middle left panel), $A_0 = 5m_0$, $\tan\beta = 20$ and $\mu > 0$ (middle right panel) and $A_0 = 3m_0$, $\tan\beta = 20$ and both positive or negative μ (lower panels) with the Higgs mass calculated using different codes: `FeynHiggs 2.10.0` (cyan lines) and `2.13.0` (purple lines), `SSARD` (green lines) and `SUSYHD` (black lines). The horizontal yellow strip corresponds to the 1σ band for the Higgs boson mass, $M_h = 125.09 \pm 0.24$ GeV [155]

In the case $A_0 = -4.2m_0$, $\mu > 0$ and $\tan\beta = 5$ (upper left panel of Fig. 3), the calculated value of M_h is always less than the experimental value, even taking the theoretical uncertainty into account. On the other hand, in the case $A_0 = -4.2m_0$, $\mu > 0$ and $\tan\beta = 5$ or $\tan\beta = 20$ (upper right and middle left panels of Fig. 3), the calculated value of M_h is compatible with the measured value all the way from $m_{1/2} \sim 3$ TeV to the end of the stop coannihilation strip at $m_{1/2} \sim 7$ TeV. Although the Higgs mass is stable, we note that the extent of the stop strip is restricted because $A_0 < 0$.

For the middle right and bottom two panels of Fig. 3, we consider $A_0 > 0$, and the stop masses are much more split and the A-terms at the SUSY scale are much larger. This extreme set of soft supersymmetry-breaking parameters makes it rather difficult to calculate the Higgs mass. Since the splitting of the stop masses along the stop coannihilation strip

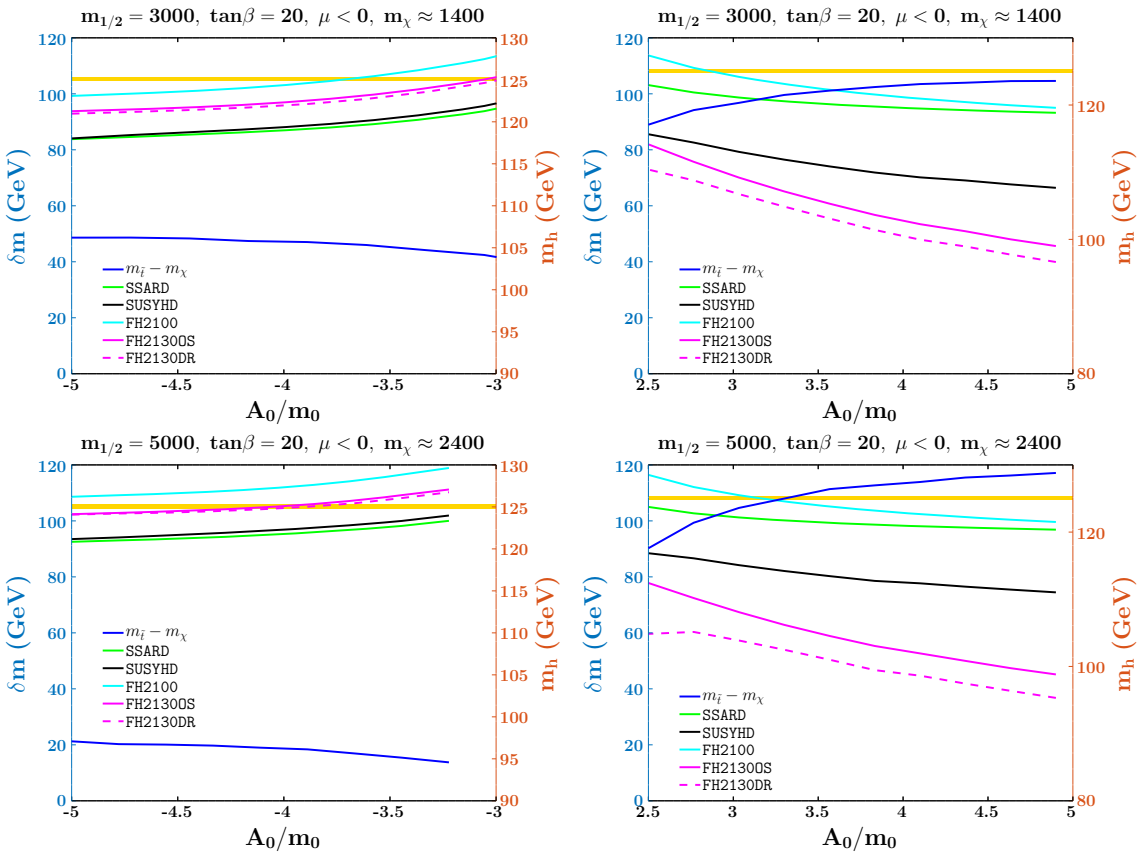

Fig. 4 Examination of Higgs mass for large A-terms along the stop coannihilation strip. The horizontal yellow strip corresponds to the 1σ band for the Higgs boson mass, $M_h = 125.09 \pm 0.24$ GeV [155]

becomes even more extreme for larger $m_{1/2}$, the variance in the Higgs mass calculators make it unclear what really is the endpoint of the stop coannihilation strip. For example, in the middle right panel, we take $A_0 = 5m_0$, $\tan\beta = 20$ and $\mu > 0$ and for the bottom left we take instead $A_0 = 3m_0$. In these panels, the Higgs mass using `FeynHiggs 2.13.0` DR goes below 70 GeV when $m_{1/2} \sim 7$ TeV. Ignoring this, the spread in the Higgs mass is still 40 GeV(35 GeV) for $A_0 = 5m_0$ ($A_0 = 3m_0$). The situation is slightly better when $\mu < 0$, where the `FeynHiggs 2.13.0` DR calculation only drops slightly below 100 GeV. In this case, the spread including the `FeynHiggs 2.13.0` DR calculation is of order 30 GeV and without it is of order 25 GeV. Although this case is better, it is still far too inaccurate to derive any meaningful constraints on the extent of the stop coannihilation strip.

In Fig. 4, we examine the Higgs mass calculators along the stop strip as a function of the input trilinear coupling A_0 for $\mu < 0$ and $\tan\beta = 20$. In the upper (lower) panel we set $m_{1/2} = 3000$ GeV ($m_{1/2} = 5000$ GeV). For the two left panels, the $A_0 < 0$ portion is shown. In this regime, the Higgs mass calculators agree reasonably well with each other over the entire range of A_0 plotted, with the variation in the Higgs mass being less than 10 GeV. The difference in the stop and LSP mass, δm, which is needed to give an acceptable dark matter relic density is of order 40 GeV (20 GeV) for the upper left (bottom left) panel. In the right two panels, we show the $A_0 > 0$ parameter space where the Higgs mass calculators do not agree. The variation in the Higgs mass calculators is around 20 GeV (25 GeV) for the upper right (bottom right) panel.

For completeness, we show two examples of $(m_{1/2}, m_0)$ planes in the CMSSM with $\tan\beta = 20$ in Fig. 5. In the left panel, we have chosen $A_0 = -3.5m_0$ and $\mu < 0$, and in the right panel, $A_0 = 2.75$ and $\mu > 0$. In both panels, the brick-shaded regions are where the LSP is charged, and are for that reason excluded by cosmology. The brick-shaded region in the lower right corner corresponds to a stau LSP, while that in the upper left corner corresponds to a stop LSP. For a given value of m_0, the stop mass varies very rapidly with $m_{1/2}$ making the stop coannihilation strip (shown in blue) extremely thin (essentially invisible) even when extending the range on the cosmological density to $0.01 < \Omega h^2 < 2$. In the left panel, the strip ends at the point marked with an X (near $(m_{1/2}, m_0) = (6.6, 14.8)$ TeV). In the right panel, the stop strip extends beyond the range shown. However, the coordinates of the end point can be surmised by examining

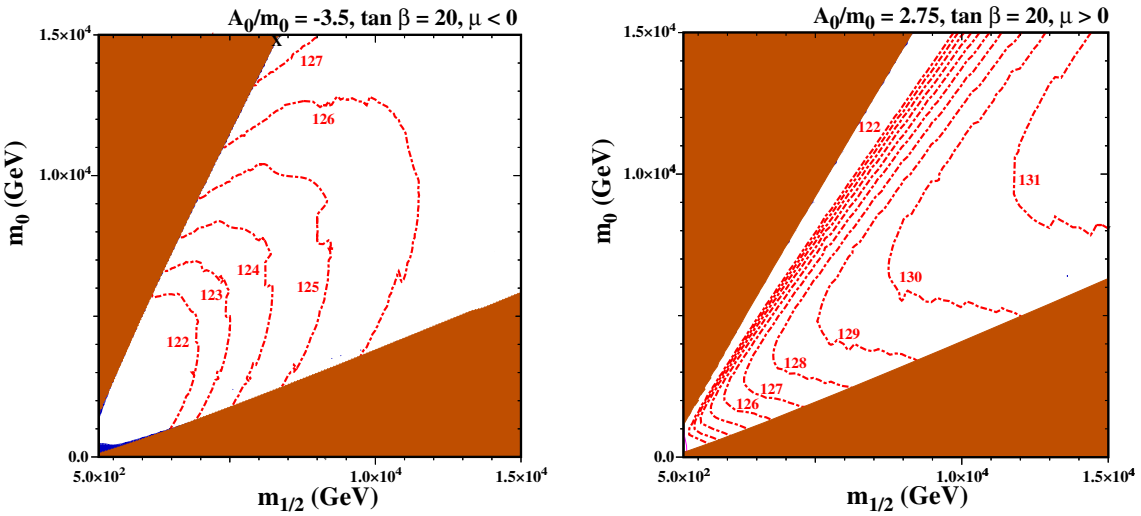

Fig. 5 The $(m_{1/2}, m_0)$ planes in the CMSSM with $\tan\beta = 20$. In the left panel, $A_0 = -3.5m_0$ and $\mu < 0$, whereas in the right panel $A_0 = 2.75m_0$ and $\mu > 0$. Strips with the allowed cosmological LSP density are shaded dark blue (enhanced so that $0.01 < \Omega h^2 < 2.0$ though they are still essentially invisible). The endpoint of the strip in the left panel is marked with an X, but is beyond the range of the right panel. Regions where the LSP is charged are shaded brick red and contours of M_h are indicated by red dot-dashed lines

Fig. 7. The most noticeable difference between the two panels is the value of the Higgs mass across the plane: contours of the Higgs mass are shown by the red dot-dashed curves. Consistent with the discussion above, the Higgs mass along the strip is reasonable only when $A_0 < 0$ and $\mu < 0$. A related discussion on similar planes can be found in [36].

5 The stop coannihilation strip in sub-GUT models

We now discuss the stop coannihilation strip in a variant of the CMSSM in which the soft supersymmetry-breaking sparticle masses are assumed to be universal at some renormalization scale $M_{\rm in} < M_{\rm GUT}$, as in 'mirage unification' [136–147] and other sub-GUT models [132,132,133]. As was commented above, one can anticipate that the stop coannihilation strip may extend to larger LSP masses than in the CMSSM, because the renormalization-group running of the input parameters over a smaller range of scales allows the two stop masses $m_{\tilde{t}_1}$ and $m_{\tilde{t}_2}$ to be more similar than in the CMSSM. Since the Higgs squared mass depends on $A_t^2/m_{\tilde{t}_1}m_{\tilde{t}_2}$ while the length of the coannihilation strip depends approximately on $A_t^2/(m_{\tilde{t}_1}^2 + m_{\tilde{t}_2}^2)$, this enables the length of the coannihilation strip to be maximized while retaining a value of the Higgs mass that is consistent with experiment.

In Fig. 6 we compare two $(m_{1/2}, m_0)$ planes in a sub-GUT model with $M_{in} = 10^9$ GeV and $\tan\beta = 20$. In the left panel, $A_0 = 2.75m_0$ and $\mu < 0$ while in the right panel $A_0 = 2.75m_0$ and $\mu > 0$. As in Fig. 5, the brick-shaded regions are where the LSP is charged. Here, the lighter stop squark is the LSP in the brick-coloured region at small $m_{1/2}$ and relatively large m_0, as well as in a diagonal band extending to large $m_{1/2}$ and m_0. In the right panel, the stop LSP region is split in two parts with the area between them having a mixed Higgsino/Bino LSP. There is a narrower band extending from $(m_{1/2}, m_0) \sim (6, 5)$ TeV to $(12, 13)$ TeV and beyond, outlined in black, where the LSP is a charged Higgsino. The chargino LSP arises because the LSP is changing from being Bino-like in the upper left corner of the figure to Higgsino-like in the lower right corner. When the Bino and Higgsino masses become degenerate, the mixing becomes significant, lifting the masses of the neutral Higgsinos and leading to a charged Higgsino LSP. Finally, at large $m_{1/2}$ and relatively small m_0 there is a region where the LSP is the lighter stau.

Above and to the right of the stop LSP region in the right panel of Fig. 6 there is a pair of blue bands where the relic neutralino LSP density falls within the range indicated by the Planck and other measurements [37]. These aim towards a vertex at $m_{1/2} \sim m_0 \sim 10$ TeV that lies, however, within the Higgsino LSP region that separates the two bands. We note in addition the appearance of an outwards-pointing spike in the upper dark matter strip, whose base is at $(m_{1/2}, m_0) \sim (8, 10)$ TeV. Along the two flanks of this spike, the dark matter density is brought down into the range allowed by cosmology by rapid $\tilde{t}_1\tilde{t}_1^*$ annihilation via the heavy Higgs bosons H in the direct channel.[11] Compared with the stop coannihilation strips in the CMSSM, these subGUT strips are relatively thick and clearly visible in the figure, even with

[11] The actual extent of the spike is unclear due to numerical uncertainties in calculating the Higgs bosons mixing angle.

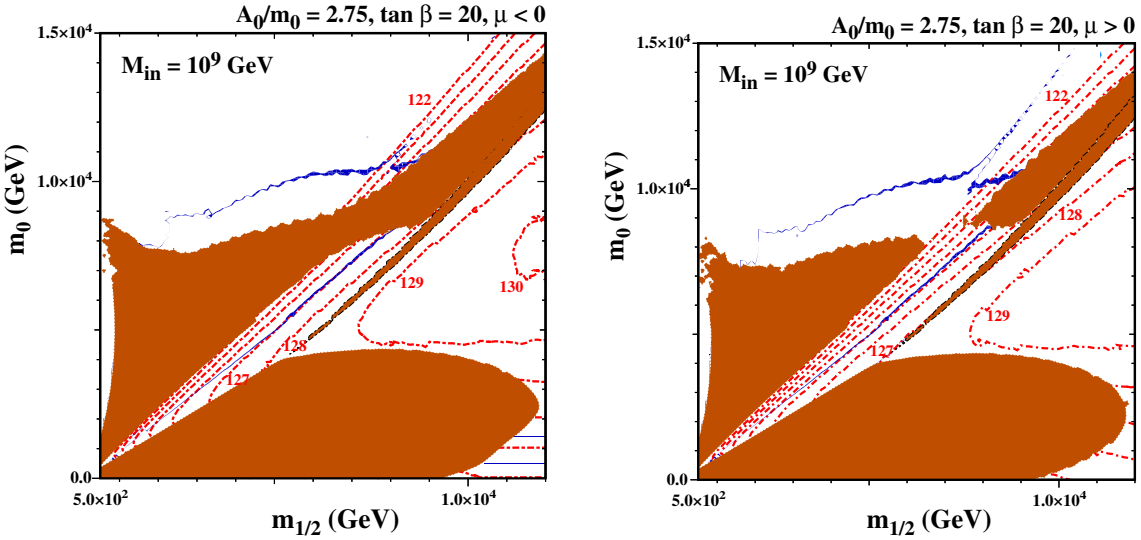

Fig. 6 The $(m_{1/2}, m_0)$ planes in a sub-GUT model with $M_{in} = 10^9$ GeV and $\tan\beta = 20$. In the left panel, $A_0 = 2.75m_0$ and $\mu < 0$, whereas in the right panel $A_0 = 2.75m_0$ and $\mu > 0$. Strips with the allowed cosmological LSP density are shaded dark blue. In this figure the 3σ Planck range $0.1151 < \Omega h^2 < 0.1235$ [37] is used. Regions where the LSP is charged are shaded brick red and contours of M_h are indicated by red dot-dashed lines

the more restrictive range shown for the dark matter relic density. Unlike the CMSSM, the mass parameters along the stop coannihilation strip in sub-GUT models are much less tuned. In the upper part of the strip (which is nearly horizontal with $m_0 \sim 10$ TeV), the difference between the stop and neutralino mass changes very slowly with increasing m_0. As a result there is a broad region between the strip and the stop LSP shaded region where the relic density is too small to account for all of the dark matter. Because the difference between the stop and neutralino mass varies slowly in this figure, the coannihilation strip is relatively thick, and here we have plotted the 3 σ Planck range rather than the extended ranges used in the other figures.

Also shown in Fig. 6 as dot-dashed red lines are contours of M_h calculated using `FeynHiggs 2.13.0`. Taking into account the uncertainty in this calculation, we see that the narrower, lower, diagonal part of the stop coannihilation strip that extends from low $(m_{1/2}, m_0)$ towards the charged Higgsino LSP region is all compatible with the LHC measurement of M_h. Some of the stop coannihilation strip between the Higgsino LSP region and the outwards-pointing spike may also be consistent with the Higgs mass, given the uncertainties in the calculations. However, for $\mu > 0$, along the spike and in the region to the left of the spike, M_h appears to be too small. The situation is improved for $\mu < 0$ as the spike may be compatible, but much of the horizontal strip still lies at low M_h. Nevertheless, since there is a great deal of uncertainty in the Higgs mass calculation, as discussed in the previous section, we cannot exclude the possibility that some portions of these parts of the stop strip might also yield an acceptable Higgs boson mass.

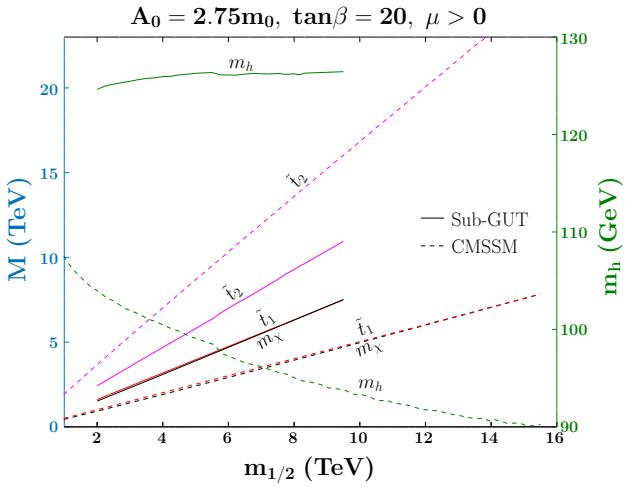

Fig. 7 The masses of the neutralino LSP, the left and right stop, and the SM like Higgs boson in the CMSSM and sub-GUT with $M_{in} = 10^9$ GeV for $A_0 = 2.75m_0$, $\tan\beta = 20$ and $sgn(\mu) > 0$

We show in Fig. 7 a comparison of relevant masses, plotted as functions of $m_{1/2}$, in the CMSSM and a sub-GUT model with $M_{in} = 10^9$ GeV, both with $A_0 = 2.75m_0$, $\tan\beta = 20$, and $\mu > 0$. The LSP mass lines are black, those for the $\tilde{t}_1$ are red, and those for the $\tilde{t}_2$ are purple. The dashed lines are for the masses in the CMSSM and the solid lines are for the sub-GUT model. In the sub-GUT case, we only plot the portion of the strip which is in between the stop and stau LSP regions. Since m_χ and $m_{\tilde{t}_1}$ depend mostly on $m_{1/2}$, their masses along the other portion of the strip just overlap the existing lines. The Higgs masses on the missing portions of the strip can

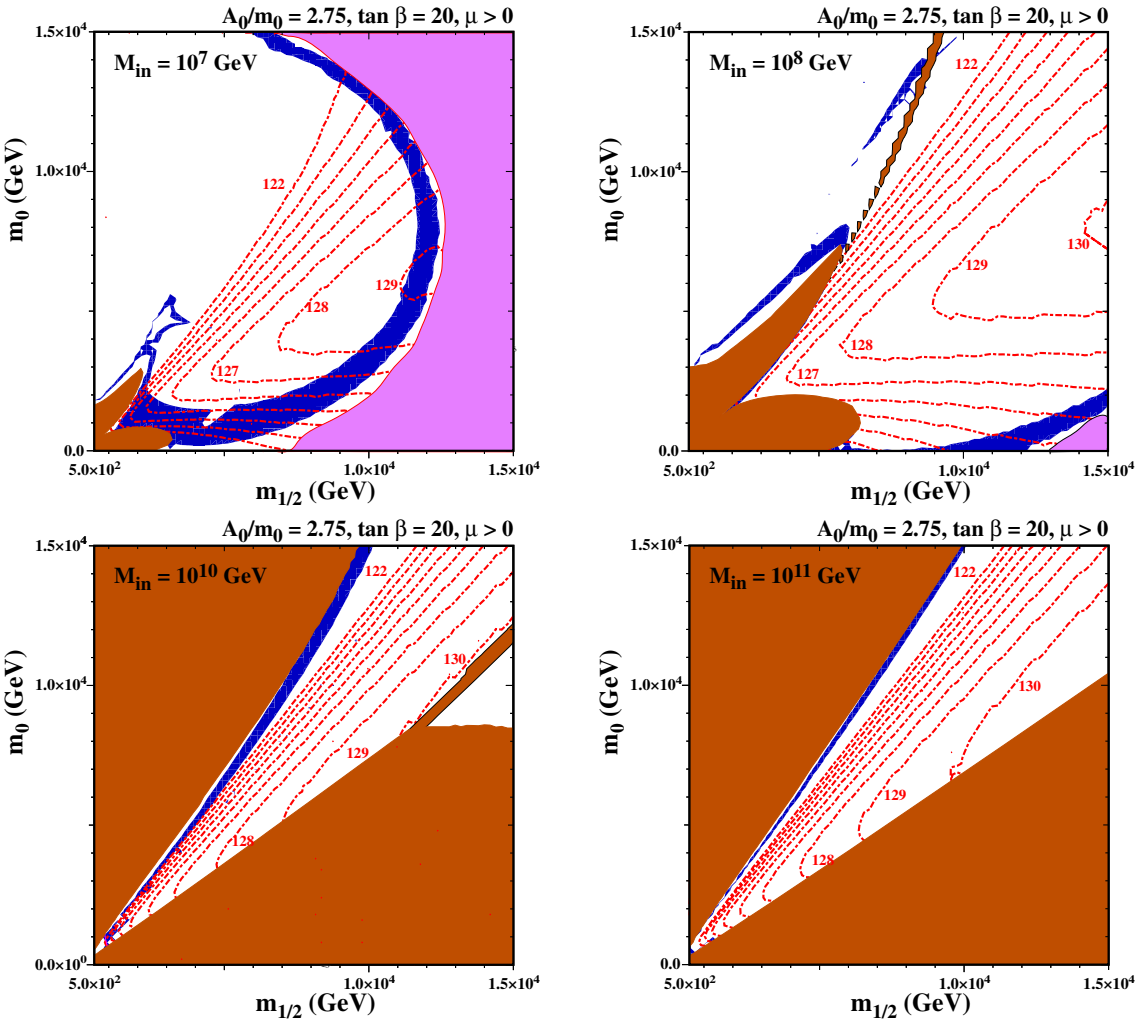

Fig. 8 The $(m_{1/2}, m_0)$ planes sub-GUT models with $\tan\beta = 20$, $A_0 = 2.75\, m_0$ and $M_{\rm in} = 10^7$ GeV (upper left), $M_{\rm in} = 10^8$ GeV (upper right), $M_{\rm in} = 10^{10}$ GeV (lower left), and $M_{\rm in} = 10^{11}$ GeV (lower right). The pink region is where $\mu^2 < 0$ and radiative EWSB is not possible. Other shadings used here are the same as Fig. 6. The shading for the relic density is enhanced so that $0.06 < \Omega h^2 < 0.2$

be inferred from Fig. 6 and tends to be too small while $m_{\tilde{t}_2}$ is slightly larger. In both the CMSSM and sub-GUT planes, the LSP, χ, and $\tilde{t}_1$ are nearly degenerate, whereas $\tilde{t}_2$ is significantly heavier. The lines are truncated at the tips of the stop strips, and the masses can be read off from the left vertical axis. As can be seen in the Figure, the Bino LSP of the sub-GUT model is much heavier than its CMSSM counterpart for the same $m_{1/2}$, but the maximum LSP masses are similar in the two cases because the strip is longer in the CMSSM case, both being ~ 7 TeV. We also see that the stop masses of the sub-GUT are much less split than in the CMSSM, which leads to a greatly enhanced Higgs boson mass.[12] For this reason, the Higgs boson mass constraint completely rules out the coannihilation strip for the CMSSM (see the dashed green line), but places no meaningful constraints on the sub-GUT model. The solid green line shows that M_h is rather insensitive to $m_{1/2}$ along the sub-GUT coannihilation strip, with a mass (to be read off the right vertical axis) that is compatible with 125 GeV within the calculational uncertainties.

We examine in Fig. 8 the impact of changing $M_{\rm in}$ on the $(m_{1/2}, m_0)$ plane in Fig. 6. We fix $\tan\beta = 20$ and $A_0 = 2.75\, m_0$ and choose $M_{\rm in} = 10^x$ GeV where $x = 7, 8, 10, 11$ for the upper left, upper right, lower left and lower right panels, respectively. In all the panels of Fig. 8 the brick-shaded region adjacent to the m_0 axis corresponds to a stop LSP, whilst in the brick-shaded region adjacent to the $m_{1/2}$ axis the LSP is a stau. For $x = 8, 10, 11$, in the brick-shaded region that is outlined in black the LSP is a charged Higgsino. In the upper panels, electroweak symmetry breaking (EWSB) is not possible in the pink regions at large $m_{1/2}$. For $M_{\rm in} = 10^7$ GeV, in the region with large $m_{1/2}$, $M_{\rm in}$ is so low that

[12] In the CMSSM for $A_0 < 0$, the Higgs mass is considerably better along the stop coannihilation strip but the extent is drastically reduced due to the smaller value of $|A|$ at the SUSY scale.

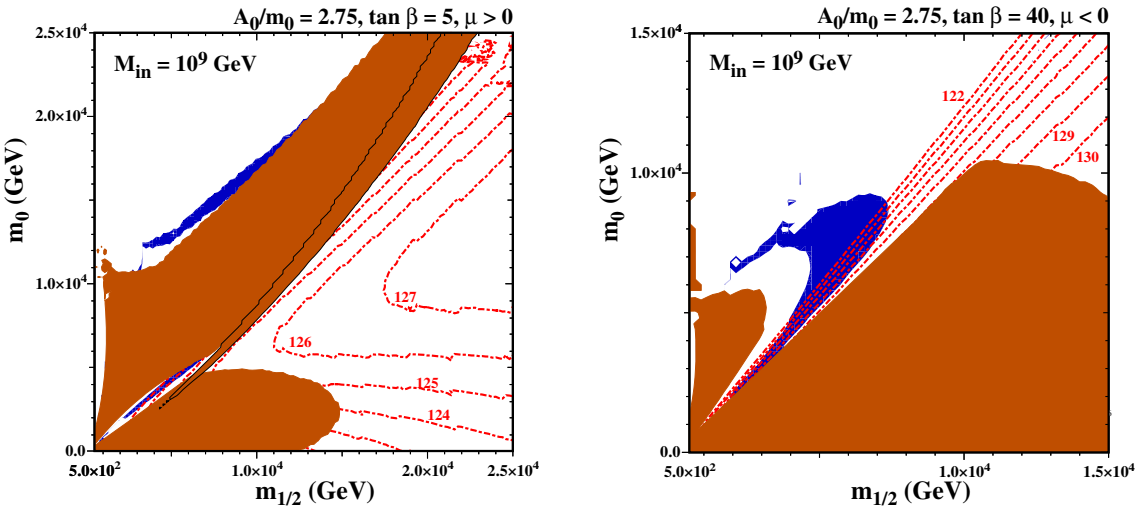

Fig. 9 The $(m_{1/2}, m_0)$ planes for sub-GUT models with $M_{\rm in} = 10^9$ GeV and $A_0 = 2.75\, m_0$, for $\tan\beta = 5$ (left panel) and $\tan\beta = 40$ (right panel). The shadings are the same as in Fig. 8

the renormalization-group running is insufficient to drive the up-type Higgs soft mass negative for large gaugino masses, so there electroweak symmetry breaking (EWSB) does not occur. The dark matter strip around the brick-shaded region that is adjacent to the m_0 axis is due to stop coannihilation, and the portion of the strip near the no-EWSB region has a typical Higgsino thermal relic with $\mu \sim 1.1$ TeV. For $M_{\rm in} = 10^8$ GeV, the stop LSP region becomes larger, extending the stop coannihilation strip to larger $m_{1/2}$ and m_0. In this case the no-EWSB region moves to larger $m_{1/2}$, and the region of parameter space with a Higgsino LSP shrinks.

Besides the strip-like regions, there is also a blue ring shape region on top of the stop strip in the panel for $M_{in} = 10^7$ GeV and a blue sliver that intersects with the chargino LSP strip seen in the panel for $M_{in} = 10^8$ GeV. In these regions of parameter space, the masses of the three lightest neutralinos are quite similar. Because of this, the χ_1, which is mostly a Bino, and the χ_2 and χ_3, which are mostly Higgsinos, can coannihilate, with an enhancement from the heavy Higgs funnel.[13] In the two panels, which have $M_{\rm in} = 10^{7,8}$ GeV, the renormalization-group running is insufficient to give a stop LSP unless $m_{1/2}$ is relatively small. Because of this, the extent of the stop coannihilation strip is greatly reduced. The maximum m_χ of the stop strips are ~ 2 GeV and 5 GeV for $M_{\rm in} = 10^{7,8}$ GeV respectively. In the panel with $M_{\rm in} = 10^{10}$ GeV, the stop LSP region has grown significantly, and is accompanied by a stop coannihilation strip that extends beyond the displayed part of the plane. The stau LSP region levels off at $m_{1/2} \sim 11$ TeV. For $M_{\rm in} = 10^{11}$ GeV, the plane has become qualitatively similar to that in the CMSSM. For $M_{\rm in} = 10^{10,11}$ GeV, the mass splitting of the stops has become large enough that the Higgs mass is suppressed to such an extent that the stop strip no longer has a viable Higgs mass and so is excluded.[14] For $M_{\rm in} = 10^9$ GeV, as seen already in Fig. 6, we are between these two extremes, and the stop LSP region is large enough to give a coannihilation strip that extends to large $m_{1/2}$, but is not so large that the Higgs boson mass becomes too small. In this case, the maximum value of m_χ in the stop strip after taking M_h into account is ~ 7.4 TeV, lying on top of the diagonal brick-shaded band in the right panel of Fig 6.

The next pair of plots examines the effect of changing $\tan\beta$. In Fig. 9 we show the $(m_{1/2}, m_0)$ planes for $M_{\rm in} = 10^9$ GeV and $A_0 = 2.75\, m_0$ for $\tan\beta = 5(40)$ in the left (right) panel. In the case with $\tan\beta = 5$ the stop LSP region has grown because of the larger top Yukawa coupling. Indeed, it has grow so much that it merges with the charged Higgsino LSP region, forcing the lower stop coannihilation strip to terminate at a much lower value of $m_{1/2} \sim 7$ TeV and $m_\chi \sim 5.4$ TeV. Within this region, M_h is compatible with 125 GeV, within the calculational uncertainties. The upper stop coannihilation strip extends farther in $m_{1/2}$ and m_0, but the Higgs mass is very low here.[15] For $\tan\beta = 40$, on the other hand, the stop LSP region has shrunk while the stau LSP region has grown. This is again due the $\tan\beta$ dependence of the Yukawa couplings. The increase in the tau Yukawa coupling is responsible for the larger stau LSP region, and the smaller top Yukawa coupling for the smaller stop LSP region. The shrinking of the stop LSP regions leads to the stop coannihilation strip terminating at much lower values

[13] Unlike the heavy Higgs funnel in Fig. 6, the extent of this funnel is not sensitive to the exact value of the Higgs mixing angle.

[14] For $\mu < 0$, the value of the Higgs mass is improved, but is still much too small to meet experimental constraints.

[15] The Higgs mass is again improved for $\mu < 0$, but is still far below the experimental constraint.

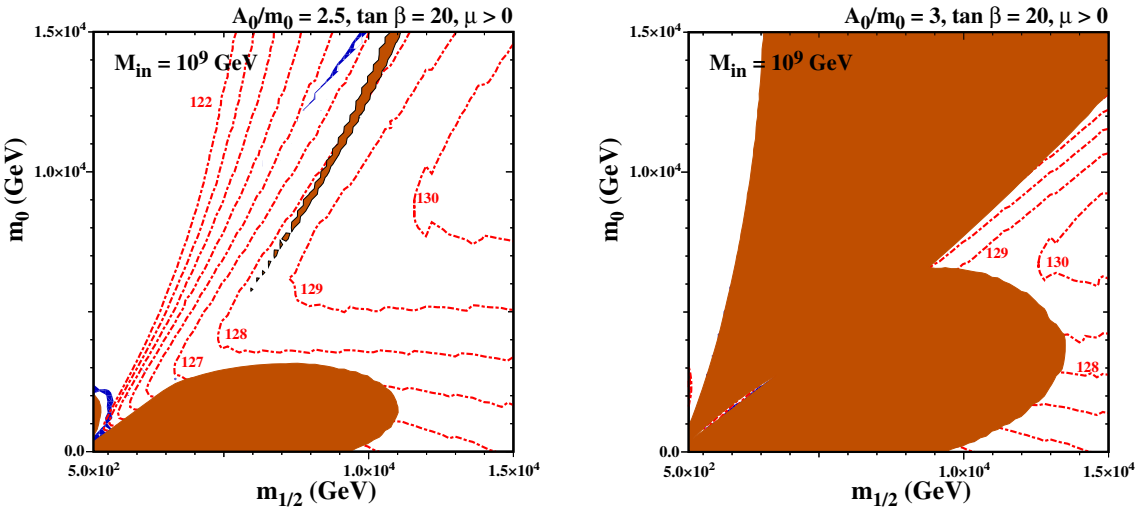

Fig. 10 The $(m_{1/2}, m_0)$ planes for sub-GUT models with $M_{\rm in} = 10^9$ GeV, $\tan\beta = 20$ and for $A_0 = 2.5\,m_0$ (left panel) and $A_0 = 3\,m_0$ (right panel). The shadings are the same as in Fig. 8

of $m_{1/2} \sim 7$ TeV and the LSP mass ~ 5.5 TeV,[16] compared with the case of a more moderate value of $\tan\beta = 20$ studied previously, which leads to a stop coannihilation strip that extends to larger LSP masses.

The last pair of plots show the effect of varying A_0. In Fig. 10 we show the $(m_{1/2}, m_0)$ planes for $M_{\rm in} = 10^9$ GeV and $\tan\beta = 20$ for $A_0 = 2.5\,m_0$ ($A_0 = 3\,m_0$) in the left (right) panel. In the left panel, the smaller A-term is unable to push the stop mass tachyonic unless $m_{1/2}$ is very small. Because of this, the stop coannihilation strip has all but disappeared, clinging on only when $m_{1/2} \lesssim 2$ TeV in a region where the value of M_h calculated using `FeynHiggs 2.13.0` is < 125 GeV. As was the case in Fig. 8, the blue sliver in the upper part of the panel appears because χ_1, χ_2, and χ_3 are nearly degenerate and have an enhanced annihilation rate to the (nearly) on-shell heavy Higgs bosons. For a larger A-term, as shown in the right panel, the stop coannihilation region grows and merges with the stau coannihilation region and charged-Higgsino strip. The parameter space no longer exhibits a stop coannihilation strip. As one can see, the spectrum at $M_{in} = 10^9$ GeV, is very sensitive to A_0/m_0, and the rich structure seen in the previous figures requires $A_0/m_0 \approx 2.75$.

6 Conclusions

It is well-known that an effective way to reduce the relic density of a massive LSP into the range allowed by Planck and other astrophysical and cosmological observations is coannihilation of the LSP with at least one other particle of similar mass that decouples at around the same time in the early universe. In this case, as long as the temperature of the thermal bath is no smaller than the difference between the particle masses, the lighter one - the LSP candidate - can scatter in the thermal bath and be converted to the heavier particle. If the heavier particle can annihilate efficiently into Standard Model particles, the relic density of the dark matter candidate can be significantly reduced. The more strongly interacting the coannihilating particle, the more efficient it is at reducing the relic density. In supersymmetric models, one of the most effective coannihilating partners for the LSP is the lighter stop. It is particularly effective because stop-antistop annihilation rates to hh and WW/ZZ are enhanced if the A-terms are large. This enhancement of the annihilations to WW/ZZ arises because the longitudinal Goldstone bosons interact with the stops through A-terms. Specifically, the amplitudes for $\tilde{t}\tilde{t}^* \to WW, ZZ, hh$ all receive an enhancement proportional to $A_t^2/(m_{\tilde{t}_R}^2 + m_{\tilde{t}_L}^2)$. On top of this enhancement, these annihilation processes are boosted by Sommerfeld enhancement and by bound state formation.

In the CMSSM, these enhanced annihilation rates of stops allow the relic density to be consistent with Planck constraints for $m_{1/2} \lesssim 17$ TeV, with an LSP mass $m_\chi \sim 8.5$ TeV. However, a Bino mass this large requires $A_0 \sim 5\,m_0$. Such a large A-term splits the stop mass eigenstates severely, leading to an unacceptably small mass for the lightest supersymmetric Higgs boson. In the CMSSM, the Higgs mass measurement places a strong constraint on the extent of the stop coannihilation strip, if the Higgs mass is calculated with `FeynHiggs 2.13.0`, the supersymmetric Higgs mass calculator we use for this study. With the Higgs mass constraint included, $A_0 \sim 5\,m_0$ is no longer viable. For $A_0/m_0 = -4.2$,

[16] Although a large portion of the coannihilation strip follows the stau LSP region, the relic density is reduced through coannihilation with the stop, which also has a similar mass to the LSP.

$\tan\beta = 5$ and $\mu > 0$, the stop coannihilation strip can only reach $m_{1/2} \sim 7.2$ TeV with an LSP mass of $m_\chi \sim 3.5$ TeV for $m_0 \sim 12$ TeV,

However, it is not clear how reliable Higgs mass calculators are in this extreme regime, and therefore how seriously one should take this constraint on the stop coannihilation strip. This concern arises from the fact that the various publicly available Higgs mass calculators yield very different results in this regime. For the CMSSM with $A_0 = 5\,m_0$, $\tan\beta = 20$ and $\mu > 0$, the Higgs mass calculators give a mass for the Standard Model-like Higgs boson that span a range of order 70 GeV. Although the spread is smaller for $A_0 < 0$, where the Higgs mass spans a range of order 10 GeV for $A_0 = -4.2m_0$, $\tan\beta = 20$ and $\mu > 0$, this regime is much less extreme and the extent of the stop coannihilation strip is drastically reduced. This is due to the fact that for $A_0 < 0$, the renormalization-group running suppresses the A-terms much more drastically as they are run down to the supersymmetry-breaking scale. With such smaller A-terms, the Higgs mass calculations become much more reliable and the annihilations $\tilde{t}\tilde{t}^* \to hh, WW, ZZ$ becomes much less effective. Because of this, the stop coannihilation strip only reaches $m_{1/2} \sim 7$ TeV and $m_\chi \sim 3.5$ TeV for $A_0 = -4.2\,m_0$, $\tan\beta = 20$ and $\mu > 0$. Thus, if the results of `FeynHiggs 2.13.0` in this regime are in fact reliable, the extent of the stop coannihilation strip in the CMSSM is drastically reduced.

However, for stop masses that are more degenerate, the Higgs mass constraints are less restrictive. In sub-GUT models, in which the soft supersymmetry-breaking masses unify at some lower scale $M_{\rm in}$, the low-scale stop masses tend to be more degenerate due to the reduced running. Because of this increased degeneracy, a Bino LSP mass of $m_\chi \sim 7$ TeV can be consistent with the Planck relic density measurement for $A_0 = 2.75\,m_0$, $\tan\beta = 20$, and $\mu > 0$ with $M_{\rm in} = 10^9$ GeV. Moreover, in this case calculations with `FeynHiggs 2.13.0` yield a mass of the lightest supersymmetric Higgs boson that is compatible with 125 GeV all the way to the tip of the stop coannihilation strip.

In addition to demonstrating that an LSP mass $m_\chi \sim 8$ TeV can be compatible with the relevant dark matter density and Higgs mass constraints in a sub-GUT model, our work highlights the importance of annihilations into the longitudinal modes of massive gauge bosons, as well as the Sommerfeld enhancement and bound-state effects. It also highlights the need for a reliable code to calculate the lightest Higgs mass in the extreme regions of parameter space that are relevant for large LSP masses. The results obtained with `FeynHiggs 2.13.0` may well be reliable in many cases, but corroboration is essential.

Acknowledgements We would like to thank S. Heinemeyer for his continuing help with our implementation of `FeynHiggs`. The work of J.E. was supported in part by STFC (UK) via the research Grant ST/L000326/1, and in part by the Estonian Research Council via a Mobilitas Pluss Grant. F.L. was supported by the World Premier International Research Center Initiative (WPI), MEXT, Japan. The work of K.A.O. was supported in part by DOE Grant DE-SC0011842 at the University of Minnesota. The work of J. Z. was supported in part by KAKENHI Grant number JP26104009.

Funded by SCOAP[3].

References

1. ATLAS Collaboration. https://twiki.cern.ch/twiki/bin/view/AtlasPublic/SupersymmetryPublicResults
2. CMS Collaboration. https://twiki.cern.ch/twiki/bin/view/CMSPublic/PhysicsResultsSUS
3. J.R. Ellis, S. Kelley, D.V. Nanopoulos, Phys. Lett. B **249**, 441 (1990)
4. J.R. Ellis, S. Kelley, D.V. Nanopoulos, Phys. Lett. B **260**, 131 (1991)
5. U. Amaldi, W. de Boer, H. Furstenau, Phys. Lett. B **260**, 447 (1991)
6. P. Langacker, M.-X. Luo, Phys. Rev. D **44**, 817 (1991)
7. C. Giunti, C.W. Kim, U.W. Lee, Mod. Phys. Lett. A **6**, 1745 (1991)
8. L. Maiani, in *Proceedings, Gif-sur-Yvette Summer School On Particle Physics*, 1–52 (1979)
9. Gerard 't Hooft, et al. (eds.), *Recent Developments in Gauge Theories, Proceedings of the Nato Advanced Study Institute, Cargese, France, August 26 - September 8, 1979* (Plenum press, New York, 1980) Nato Advanced Study Institutes Series: Series B, Physics, pp. 59
10. E. Witten, Phys. Lett. B **105**, 267 (1981)
11. H. Goldberg, Phys. Rev. Lett. **50**, 1419 (1983)
12. J. Ellis, J. Hagelin, D. Nanopoulos, K. Olive, M. Srednicki, Nucl. Phys. B **238**, 453 (1984)
13. J.R. Ellis, D. Ross, Phys. Lett. B **506**, 331 (2001). arXiv:hep-ph/0012067
14. D. Buttazzo, G. Degrassi, P.P. Giardino, G.F. Giudice, F. Sala, A. Salvio, A. Strumia, JHEP **1312**, 089 (2013). arXiv:1307.3536 [hep-ph]
15. G. Degrassi, S. Di Vita, J. Elias-Miro, J.R. Espinosa, G.F. Giudice, G. Isidori, A. Strumia, JHEP **1208**, 098 (2012). arXiv:1205.6497 [hep-ph]
16. L.E. Ibanez, G.G. Ross, Phys. Lett. B **110**, 215 (1982)
17. K. Inoue, A. Kakuto, H. Komatsu and S. Takeshita, Prog. Theor. Phys. **68**, 927 (1982) [Erratum-ibid. **70**, 330 (1983)] [Prog. Theor. Phys. **70**, 330 (1983)]
18. L.E. Ibanez, Phys. Lett. B **118**, 73 (1982)
19. J.R. Ellis, D.V. Nanopoulos, K. Tamvakis, Phys. Lett. B **121**, 123 (1983)
20. J.R. Ellis, J.S. Hagelin, D.V. Nanopoulos, K. Tamvakis, Phys. Lett. B **125**, 275 (1983)
21. L. Alvarez-Gaume, J. Polchinski, M.B. Wise, Nucl. Phys. B **221**, 495 (1983)
22. J.R. Ellis, G. Ridolfi, F. Zwirner, Phys. Lett. B **257**, 83 (1991)
23. J.R. Ellis, G. Ridolfi, F. Zwirner, Phys. Lett. B **262**, 477 (1991)
24. Y. Okada, M. Yamaguchi, T. Yanagida, Prog. Theor. Phys. **85**, 1 (1991)

25. A. Yamada, Phys. Lett. B **263**, 233 (1991)
26. Howard E. Haber, Ralf Hempfling, Phys. Rev. Lett. **66**, 1815 (1991)
27. M. Drees, M.M. Nojiri, Phys. Rev. D **45**, 2482 (1992)
28. P.H. Chankowski, S. Pokorski, J. Rosiek, Phys. Lett. B **274**, 191 (1992)
29. P.H. Chankowski, S. Pokorski, J. Rosiek, Phys. Lett. B **286**, 307 (1992)
30. J.R. Ellis, D.V. Nanopoulos, K.A. Olive, Y. Santoso, Phys. Lett. B **633**, 583 (2006). arXiv:hep-ph/0509331
31. V. Takhistov [for the Super-Kamiokande Collaboration]. arXiv:1605.03235 [hep-ex]
32. T. Goto, T. Nihei, Phys. Rev. D **59**, 115009 (1999). arXiv:hep-ph/9808255
33. H. Murayama, A. Pierce, Phys. Rev. D **65**, 055009 (2002). arXiv:hep-ph/0108104
34. J.L. Evans, N. Nagata, K.A. Olive, Phys. Rev. D **91**, 055027 (2015). arXiv:1502.00034 [hep-ph]
35. J. Ellis, J.L. Evans, F. Luo, N. Nagata, K.A. Olive, P. Sandick, Eur. Phys. J. C **76**(1), 8 (2016). arXiv:1509.08838
36. J. Ellis, J.L. Evans, A. Mustafayev, N. Nagata, K.A. Olive, Eur. Phys. J. C **76**(11), 592 (2016). arXiv:1608.05370
37. P.A.R. Ade et al., Planck Collaboration. Astron. Astrophys. **594**, A13 (2016). https://doi.org/10.1051/0004-6361/201525830. arXiv:1502.01589 [astro-ph.CO]
38. K. Griest, D. Seckel, Phys. Rev. D **43**, 3191 (1991)
39. J. Ellis, T. Falk, K.A. Olive, Phys. Lett. B **444**, 367 (1998). arXiv:hep-ph/9810360
40. J. Ellis, T. Falk, K.A. Olive, and M. Srednicki, *Astr. Part. Phys.***13**, 181 (2000) [Erratum-ibid. **15**, 413 (2001)]. arXiv:hep-ph/9905481
41. R. Arnowitt, B. Dutta, Y. Santoso, Nucl. Phys. B **606**, 59 (2001). arXiv:hep-ph/0102181
42. M.E. Gómez, G. Lazarides, C. Pallis, Phys. Rev. D **D61**, 123512 (2000). arXiv:hep-ph/9907261
43. M.E. Gómez, G. Lazarides, C. Pallis, Phys. Lett. B **487**, 313 (2000). arXiv:hep-ph/0004028
44. M.E. Gómez, G. Lazarides, C. Pallis, Nucl. Phys. B **B638**, 165 (2002). arXiv:hep-ph/0203131
45. T. Nihei, L. Roszkowski, R. Ruiz de Austri, JHEP **0207**, 024 (2002)
46. M. Citron, J. Ellis, F. Luo, J. Marrouche, K. A. Olive and K. J. de Vries, Phys. Rev. D **87**(3), 036012 (2013). arXiv:1212.2886 [hep-ph] and references therein
47. N. Desai, J. Ellis, F. Luo, J. Marrouche, Phys. Rev. D **90**(5), 055031 (2014). arXiv:1404.5061 [hep-ph]
48. S. Mizuta, M. Yamaguchi, Phys. Lett. B **298**, 120 (1993). arXiv:hep-ph/9208251
49. J. Edsjö, P. Gondolo, Phys. Rev. D **56**, 1879 (1997). arXiv:hep-ph/9704361
50. H. Baer, C. Balazs, A. Belyaev, JHEP **0203**, 042 (2002). arXiv:hep-ph/0202076
51. A. Birkedal-Hansen, E.H. Jeong, JHEP **0302**, 047 (2003). arXiv:hep-ph/0210041
52. C. Boehm, A. Djouadi, M. Drees, Phys. Rev. D **62**, 035012 (2000). arXiv:hep-ph/9911496
53. J.R. Ellis, K.A. Olive, Y. Santoso, Astropart. Phys. **18**, 395 (2003). arXiv:hep-ph/0112113
54. J.L. Diaz-Cruz, J.R. Ellis, K.A. Olive, Y. Santoso, JHEP **0705**, 003 (2007). arXiv:hep-ph/0701229
55. I. Gogoladze, S. Raza, Q. Shafi, Phys. Lett. B **706**, 345 (2012). arXiv:1104.3566 [hep-ph]
56. M.A. Ajaib, T. Li, Q. Shafi, Phys. Rev. D **85**, 055021 (2012). arXiv:1111.4467 [hep-ph]
57. J. Harz, B. Herrmann, M. Klasen, K. Kovarik, Q.L. Boulc'h, Phys. Rev. D **87**(5), 054031 (2013). arXiv:1212.5241
58. J. Harz, B. Herrmann, M. Klasen, K. Kovarik, Phys. Rev. D **91**(3), 034028 (2015). arXiv:1409.2898 [hep-ph]
59. A. Ibarra, A. Pierce, N.R. Shah, S. Vogl, Phys. Rev. D **91**(9), 095018 (2015). arXiv:1501.03164 [hep-ph]
60. J. Edsjö, M. Schelke, P. Ullio, P. Gondolo, JCAP **0304**, 001 (2003). arXiv:hep-ph/0301106
61. J. Ellis, K.A. Olive, J. Zheng, Eur. Phys. J. C **74**, 2947 (2014). arXiv:1404.5571 [hep-ph]
62. O. Buchmueller, M. Citron, J. Ellis, S. Guha, J. Marrouche, K.A. Olive, K. de Vries, J. Zheng, Eur. Phys. J. C **75**(10), 469 (2015). arXiv:1505.04702 [hep-ph]
63. S. Raza, Q. Shafi, C.S. Ün, Phys. Rev. D **92**(5), 055010 (2015). arXiv:1412.7672 [hep-ph]
64. S. Profumo, C.E. Yaguna, Phys. Rev. D **69**, 115009 (2004). arXiv:hep-ph/0402208
65. D. Feldman, Z. Liu, P. Nath, Phys. Rev. D **80**, 015007 (2009). arXiv:0905.1148 [hep-ph]
66. N. Chen, D. Feldman, Z. Liu, P. Nath, G. Peim, Phys. Rev. D **83**, 035005 (2011). arXiv:1011.1246 [hep-ph]
67. I. Gogoladze, R. Khalid, Q. Shafi, Phys. Rev. D **79**, 115004 (2009). arXiv:0903.5204 [hep-ph]
68. I. Gogoladze, R. Khalid, Q. Shafi, Phys. Rev. D **80**, 095016 (2009). arXiv:0908.0731 [hep-ph]
69. M. Adeel Ajaib, T. Li, Q. Shafi, K. Wang, JHEP **1101**, 028 (2011). arXiv:1011.5518 [hep-ph]
70. K. Harigaya, M. Ibe, T.T. Yanagida, JHEP **1312**, 016 (2013). arXiv:1310.0643 [hep-ph]
71. K. Harigaya, K. Kaneta, S. Matsumoto, Phys. Rev. D **89**(11), 115021 (2014). arXiv:1403.0715 [hep-ph]
72. J.L. Evans, K.A. Olive, Phys. Rev. D **90**(11), 115020 (2014). arXiv:1408.5102 [hep-ph]
73. A. De Simone, G.F. Giudice, A. Strumia, JHEP **1406**, 081 (2014). arXiv:1402.6287 [hep-ph]
74. M. Low, L.T. Wang, JHEP **1408**, 161 (2014). arXiv:1404.0682 [hep-ph]
75. J. Ellis, F. Luo, K.A. Olive, JHEP **1509**, 127 (2015). arXiv:1503.07142 [hep-ph]
76. J. Ellis, J.L. Evans, F. Luo, K.A. Olive, JHEP **1602**, 071 (2016). https://doi.org/10.1007/JHEP02(2016)071. arXiv:1510.03498 [hep-ph]
77. K.A. Olive, M. Srednicki, Phys. Lett. B **230**, 78 (1989)
78. K.A. Olive, M. Srednicki, Nucl. Phys. B **355**, 208 (1991)
79. J. Hisano, S. Matsumoto, M. Nagai, O. Saito, M. Senami, Phys. Lett. B **646**, 34 (2007). arXiv:hep-ph/0610249
80. M. Cirelli, A. Strumia, M. Tamburini, Nucl. Phys. B **787**, 152 (2007). arXiv:0706.4071 [hep-ph]
81. A. Hryczuk, R. Iengo, P. Ullio, JHEP **1103**, 069 (2011). arXiv:1010.2172
82. M. Beneke, A. Bharucha, F. Dighera, C. Hellmann, A. Hryczuk, S. Recksiegel, P. Ruiz-Femenia, JHEP **1603**, 119 (2016). arXiv:1601.04718 [hep-ph]
83. A. Sommerfeld, Ann. Phys. **403**, 257 (1931)
84. J. Hisano, S. Matsumoto, M.M. Nojiri, Phys. Rev. Lett. **92**, 031303 (2004). arXiv:hep-ph/0307216
85. J.L. Feng, M. Kaplinghat, H.B. Yu, Phys. Rev. D **82**, 083525 (2010). arXiv:1005.4678 [hep-ph]
86. A. Hryczuk, Phys. Lett. B **699**, 271 (2011). arXiv:1102.4295 [hep-ph]
87. J.L. Feng, M. Kaplinghat, H. Tu, H.B. Yu, JCAP **0907**, 004 (2009). arXiv:0905.3039 [hep-ph]
88. B. von Harling, K. Petraki, JCAP **1412**, 033 (2014). arXiv:1407.7874 [hep-ph]
89. K. Petraki, M. Postma, M. Wiechers, JHEP **1506**, 128 (2015). arXiv:1505.00109 [hep-ph]
90. S. Kim, M. Laine, JHEP **1607**, 143 (2016). arXiv:1602.08105 [hep-ph]

91. S. Kim, M. Laine, JCAP **1701**, 013 (2017). arXiv:1609.00474 [hep-ph]
92. K. Petraki, M. Postma, J. de Vries, JHEP **1704**, 077 (2017). arXiv:1611.01394 [hep-ph]
93. S. Biondini and M. Laine. arXiv:1801.05821 [hep-ph]
94. S.P. Liew, F. Luo, JHEP **1702**, 091 (2017). arXiv:1611.08133 [hep-ph]
95. A. Mitridate, M. Redi, J. Smirnov, A. Strumia, JCAP **1705**(05), 006 (2017). arXiv:1702.01141 [hep-ph]
96. W.Y. Keung, I. Low, Y. Zhang, Phys. Rev. D **96**(1), 015008 (2017). arXiv:1703.02977 [hep-ph]
97. G. Aad et al., ATLAS and CMS Collaborations. Phys. Rev. Lett. **114**, 191803 (2015). arXiv:1503.07589 [hep-ex]
98. S. Heinemeyer, W. Hollik, G. Weiglein, Comput. Phys. Commun. **124**, 76 (2000). arXiv:hep-ph/9812320
99. S. Heinemeyer, W. Hollik, G. Weiglein, Eur. Phys. J. C **9**, 343 (1999). arXiv:hep-ph/9812472
100. M. Frank et al., JHEP **0702**, 047 (2007). arXiv:hep-ph/0611326
101. T. Hahn, S. Heinemeyer, W. Hollik, H. Rzehak, G. Weiglein, Comput. Phys. Commun. **180**, 1426 (2009)
102. T. Hahn, S. Heinemeyer, W. Hollik, H. Rzehak and G. Weiglein, Phys. Rev. Lett. **112**(14), 141801 (2014). arXiv:1312.4937 [hep-ph]. See http://www.feynhiggs.de
103. J. Pardo Vega, G. Villadoro, JHEP **1507**, 159 (2015). arXiv:1504.05200 [hep-ph]
104. Information about this code is available from K. A. Olive: it contains important contributions from J. Evans, T. Falk, A. Ferstl, G. Ganis, F. Luo, A. Mustafayev, J. McDonald, K. A. Olive, P. Sandick, Y. Santoso, V. Spanos, M. Srednicki, and J. Zheng
105. M. Drees, M.M. Nojiri, Phys. Rev. D **47**, 376 (1993). arXiv:hep-ph/9207234
106. H. Baer, M. Brhlik, Phys. Rev. D **53**, 597 (1996). arXiv:hep-ph/9508321
107. H. Baer, M. Brhlik, Phys. Rev. D **57**, 567 (1998). arXiv:hep-ph/9706509
108. H. Baer, M. Brhlik, M.A. Diaz, J. Ferrandis, P. Mercadante, P. Quintana, X. Tata, Phys. Rev. D **63**, 015007 (2001). arXiv:hep-ph/0005027
109. J.R. Ellis, T. Falk, G. Ganis, K.A. Olive, M. Srednicki, Phys. Lett. B **510**, 236 (2001). arXiv:hep-ph/0102098
110. G.L. Kane, C.F. Kolda, L. Roszkowski, J.D. Wells, Phys. Rev. D **49**, 6173 (1994). arXiv:hep-ph/9312272
111. J.R. Ellis, T. Falk, K.A. Olive, M. Schmitt, Phys. Lett. B **388**, 97 (1996). arXiv:hep-ph/9607292
112. J.R. Ellis, T. Falk, K.A. Olive, M. Schmitt, Phys. Lett. B **413**, 355 (1997). arXiv:hep-ph/9705444
113. V.D. Barger, C. Kao, Phys. Rev. D **57**, 3131 (1998). arXiv:hep-ph/9704403
114. L. Roszkowski, R. Ruiz de Austri, T. Nihei, JHEP **0108**, 024 (2001). arXiv:hep-ph/0106334
115. A. Djouadi, M. Drees, J.L. Kneur, JHEP **0108**, 055 (2001). arXiv:hep-ph/0107316
116. U. Chattopadhyay, A. Corsetti, P. Nath, Phys. Rev. D **66**, 035003 (2002). arXiv:hep-ph/0201001
117. J.R. Ellis, K.A. Olive, Y. Santoso, New Jour. Phys. **4**, 32 (2002). arXiv:hep-ph/0202110
118. H. Baer, C. Balazs, A. Belyaev, J.K. Mizukoshi, X. Tata, Y. Wang, JHEP **0207**, 050 (2002). arXiv:hep-ph/0205325
119. R. Arnowitt and B. Dutta. arXiv:hep-ph/0211417
120. J.R. Ellis, T. Falk, G. Ganis, K.A. Olive, M. Schmitt, Phys. Rev. D **58**, 095002 (1998). arXiv:hep-ph/9801445
121. J.R. Ellis, T. Falk, G. Ganis, K.A. Olive, Phys. Rev. D **62**, 075010 (2000). arXiv:hep-ph/0004169
122. J.R. Ellis, K.A. Olive, Y. Santoso, V.C. Spanos, Phys. Lett. B **565**, 176 (2003). arXiv:hep-ph/0303043
123. H. Baer, C. Balazs, JCAP **0305**, 006 (2003). arXiv:hep-ph/0303114
124. A.B. Lahanas, D.V. Nanopoulos, Phys. Lett. B **568**, 55 (2003). arXiv:hep-ph/0303130
125. U. Chattopadhyay, A. Corsetti, P. Nath, Phys. Rev. D **68**, 035005 (2003). arXiv:hep-ph/0303201
126. C. Munoz, Int. J. Mod. Phys. A **19**, 3093 (2004). arXiv:hep-ph/0309346
127. R. Arnowitt, B. Dutta and B. Hu. arXiv:hep-ph/0310103
128. J. Ellis and K. A. Olive. arXiv:1001.3651 [astro-ph.CO], published in *Particle dark matter*, ed. G. Bertone, pp. 142–163
129. J. Ellis, K.A. Olive, Eur. Phys. J. C **72**, 2005 (2012). arXiv:1202.3262 [hep-ph]
130. O. Buchmueller et al., Eur. Phys. J. C **74**(3), 2809 (2014). arXiv:1312.5233 [hep-ph]
131. J. Ellis, F. Luo, K.A. Olive, P. Sandick, Eur. Phys. J. C **73**(4), 2403 (2013). arXiv:1212.4476 [hep-ph]
132. J.R. Ellis, K.A. Olive, P. Sandick, Phys. Lett. B **642**, 389 (2006). arXiv: hep-ph/0607002
133. J.R. Ellis, K.A. Olive, P. Sandick, JHEP **0706**, 079 (2007). arXiv:0704.3446 [hep-ph]
134. J.R. Ellis, K.A. Olive, P. Sandick, JHEP **0808**, 013 (2008). arXiv:0801.1651 [hep-ph]
135. J. C. Costa et al. arXiv:1711.00458 [hep-ph]
136. C. Csaki, in M. Shifman et al. (eds.), *From fields to strings*, vol. 2, pp. 967–1060. arXiv:hep-ph/0404096
137. K. Choi, A. Falkowski, H.P. Nilles, M. Olechowski, Nucl. Phys. B **718**, 113 (2005). arXiv:hep-th/0503216
138. K. Choi, K.S. Jeong, K.I. Okumura, JHEP **0509**, 039 (2005). arXiv:hep-ph/0504037
139. M. Endo, M. Yamaguchi, K. Yoshioka, Phys. Rev. D **72**, 015004 (2005). arXiv:hep-ph/0504036
140. A. Falkowski, O. Lebedev, Y. Mambrini, JHEP **0511**, 034 (2005). arXiv:hep-ph/0507110
141. R. Kitano, Y. Nomura, Phys. Lett. B **631**, 58 (2005). arXiv:hep-ph/0509039
142. R. Kitano, Y. Nomura, Phys. Rev. D **73**, 095004 (2006). arXiv:hep-ph/0602096
143. A. Pierce, J. Thaler, JHEP **0609**, 017 (2006). arXiv:hep-ph/0604192
144. K. Kawagoe and M. M. Nojiri. arXiv:hep-ph/0606104
145. H. Baer, E.-K. Park, X. Tata, T.T. Wang, JHEP **0608**, 041 (2006). arXiv:hep-ph/0604253
146. K. Choi, K.Y. Lee, Y. Shimizu, Y.G. Kim, K.I. Okumura, JCAP **0612**, 017 (2006). arXiv:hep-ph/0609132
147. O. Lebedev, V. Lowen, Y. Mambrini, H.P. Nilles, M. Ratz, JHEP **0702**, 063 (2007). arXiv:hep-ph/0612035
148. J.M. Cornwall, D.N. Levin, G. Tiktopoulos, Phys. Rev. D **10**, 1145 (1974) Erratum: [Phys. Rev. D 11, 972 (1975)]
149. C.E. Vayonakis, Lett. Nuovo Cim. **17**, 383 (1976)
150. M.S. Chanowitz, M.K. Gaillard, Nucl. Phys. B **261**, 379 (1985)
151. J. Harz, B. Herrmann, M. Klasen, K. Kovarik, M. Meinecke, Phys. Rev. D **91**(3), 034012 (2015). arXiv:1410.8063 [hep-ph]
152. N. Bernal, A. Djouadi, P. Slavich, JHEP **0707**, 016 (2007). arXiv:0705.1496 [hep-ph]
153. G.F. Giudice, A. Strumia, Nucl. Phys. B **858**, 63 (2012). arXiv:1108.6077 [hep-ph]
154. E. Bagnaschi, G.F. Giudice, P. Slavich, A. Strumia, JHEP **1409**, 092 (2014). arXiv:1407.4081 [hep-ph]
155. C. Patrignani et al. [Particle Data Group], Chin. Phys. C **40**(10), 100001 (2016). https://doi.org/10.1088/1674-1137/40/10/100001